The Cryosphere

EGU Open Access

Brief communication: Preliminary ICESat-2 (Ice, Cloud and land Elevation Satellite-2) measurements of outlet glaciers reveal heterogeneous patterns of seasonal dynamic thickness change

Christian J. Taubenberger[1,2], **Denis Felikson**[1,3], **and Thomas Neumann**[1]

[1]Cryospheric Sciences Laboratory, NASA Goddard Space Flight Center, Greenbelt, MD 20771, United States of America
[2]Department of Environmental Health and Engineering, Johns Hopkins University, Baltimore,
MD 21218, United States of America
[3]Goddard Earth Sciences Technology and Research Studies and Investigations II,
Morgan State University, Baltimore, MD 21251, United States of America

Correspondence: Christian J. Taubenberger (ctaubenberger@gmail.com)

Abstract. Dynamic changes of marine-terminating outlet glaciers are projected to be responsible for about half of future ice loss from the Greenland Ice Sheet. However, we lack a unified, process-based understanding that can explain the observed dynamic changes of all outlet glaciers. Many glaciers undergo seasonal dynamic thickness changes, and classifying the patterns of seasonal thickness change can improve our understanding of the processes that drive glacier behavior. The Ice, Cloud and land Elevation Satellite-2 (ICESat-2) provides space-based, seasonally repeating altimetry measurements of the ice sheets, allowing us to quantify near-termini seasonal dynamic thickness patterns of 37 outlet glaciers around the Greenland Ice Sheet. We classify the glaciers into seven common patterns of seasonal thickness change over a 2-year period from 2019 to 2020. We find small groupings of neighboring glaciers with similar patterns of seasonal thickness change, but, within larger sectors of the ice sheet, patterns of seasonal thickness change are mostly heterogeneous. Future studies can build upon our results by extending these time series, comparing seasonal dynamic thickness changes with external forcings, such as ocean temperature and meltwater runoff, and with other dynamic variables such as seasonal glacier velocity and terminus position changes.

1 Introduction

Understanding the complex nature of Earth's ice sheets is of critical importance, as they have undergone dynamic changes in recent decades (Church et al., 2013; Oppenheimer et al., 2019). Greenland Ice Sheet (GrIS) marine-terminating outlet glaciers, which drive dynamic ice mass change, are projected to account for $50 \pm 20\%$ of the total mass loss over the 21st century (Choi et al., 2021). While multi-year and decadal changes of ice sheet discharge via outlet glaciers have been studied before (Mouginot et al., 2019), patterns of seasonal thickness change have not yet been studied for a representative sample of GrIS outlet glaciers. Outlet glaciers exhibit seasonal fluctuations in velocity with distinct patterns (Moon et al., 2014; Vijay et al., 2019, 2021), but the lack of measurements of seasonal thickness change contributes to a lack of understanding of what processes control glacier dynamics on seasonal timescales. Seasonal thickness changes of outlet glaciers are driven by both external forcings (e.g., precipitation, evaporation, runoff, and terminus melt) and internal glacier dynamics (e.g., subglacial and englacial hydrology and terminus calving), and classifying their patterns of seasonal thickness change is the first step towards a more holistic understanding of the processes that control them. Prior work has used satellite altimetry to study seasonal surface elevation changes of the ice sheet (e.g., Johannessen et al., 2005; McMillian et al., 2016; Sutterley et al., 2018; Gray et al., 2019). Here, we focus on measuring dynamic ice sheet

thickness changes near the termini of 37 GrIS outlet glaciers at seasonal resolution using the ATL06 (ATLAS/ICESat-2 L3A Land Ice Height; Advanced Topographic Laser Altimeter System) land-ice along-track altimetry dataset from the Ice, Cloud and land Elevation Satellite-2 (ICESat-2; Markus et al., 2017; Neumann et al., 2019). Large-scale observational studies such as this allow for smaller, less well-studied glaciers to be observed at the same time as more well-studied glaciers and comparisons to be drawn into how these lesser-known glaciers compare with the seasonal thinning of larger glaciers, which is critical for better understanding the drivers of dynamic change in a changing climate across all outlet glaciers. We use each glacier's temporal pattern of seasonal dynamic thickness changes to group glaciers into seven distinct patterns over 2019 and 2020. We use the spatial distribution of glacier patterns to investigate whether they can be attributed to atmospheric forcing, with the hypothesis that glaciers exhibit similar seasonal patterns within regions on the order of several hundreds of kilometers, commensurate with mesoscale atmospheric-circulation patterns. Given that we present just 1 to 2 years of data, our results are not intended to definitively characterize these glaciers but, rather, to present a method for quantifying seasonal dynamic thickness changes and to highlight the heterogeneity exhibited by these glaciers over the study time period. We discuss ways in which future work could build on our results in Sect. 4.

2   Data and methods

We used three data sources within this study: (1) the ATLAS/ICESat-2 L3A Land Ice Height, Version 3 (ATL06) data product, acquired by the Advanced Topographic Laser Altimeter System (ATLAS) instrument on board the ICESat-2 observatory, which provides geolocated measurements of land-ice surface heights (Smith et al., 2019); (2) the Making Earth System Data Records for Use in Research Environments (MEaSUREs) glacier termini dataset of annual Greenland outlet glacier locations from synthetic-aperture radar (SAR) mosaics and Landsat 8 Operational Land Imager (OLI) imagery, version 1 (Joughin et al., 2015, 2017), from which we use outlet glacier locations and identifier (ID) numbers; and (3) the Arctic digital elevation model mosaic (ArcticDEM; Porter et al., 2018), a digital surface elevation model of the GrIS that we used as a reference height dataset to remove along- and across-track surface slopes from the ATL06 measurements.

ATL06 provides measurements of ice sheet surface elevation at an along-track spatial resolution of 20 m, which allows for ample spatial sampling of the fast-flowing, dynamic portions of GrIS outlet glaciers (Smith et al., 2020). We use elevation data (h_li) retrieved from all six ATLAS ground tracks to achieve the highest density of data available. ICESat-2 has a repeat cycle of 91 d, allowing for sufficient temporal sampling to measure seasonal changes of

glaciers, although we do not receive data from every satellite pass due to cloud interference. We filter out poor-quality ATL06 height data using the ATL06 quality summary flag (atl06_quality_summary), keeping only data for which the flag is set to zero.

The MEaSUREs glacier termini dataset contains locations for 238 glaciers across the GrIS, as well as an ID number (Joughin et al., 2015, 2017). We selected 65 glaciers from the MEaSUREs dataset due to their spatial distribution across several GrIS regions and a range of average ice velocities between 68 and 8141 m yr^{-1} (Rignot and Mouginot, 2012). The 65 glaciers chosen for this study also correspond to the glaciers for which a dense record of terminus positions has been generated by the Calving Front Machine (CALFIN; Cheng et al., 2021). The CALFIN dataset is currently the only pan-Greenland dataset of seasonal terminus positions. Although we do not use this dataset in this study, due to the fact that currently available CALFIN data do not extend past mid-2019, our selection of glaciers will enable comparisons of seasonal thickness change with seasonal terminus position in future studies. We define glacier seasons by 3-month periods of winter (December–January–February), spring (March–April–May), summer (June–July–August), and autumn (September–October–November). We removed glaciers that do not contain a full year (four seasons) of ICESat-2 data from either 2019 or 2020, reducing the number of glaciers categorized to 42 (listed in the Supplement).

To collect ATL06 measurements representative of near-terminus glacier thickness change, we created a 2 km × 2 km bounding box for each glacier, centered on each glacier's location in the MEaSUREs dataset, within which we aggregated ATL06 data. We manually adjusted the MEaSUREs glacier locations slightly to ensure that between one and three ICESat-2 repeat ground tracks intersect each box, but we kept each bounding box within 10 km of the terminus for each glacier. The 4 km^2 bounding box was chosen as an arbitrary size; however it was kept to this size, as a larger box may include data off the main fast-flowing section of the outlet glacier.

The ArcticDEM mosaic represents the mean ice sheet surface elevation between ca. 2015 and 2016 (Porter et al., 2018). The DEM has a 32 m spatial resolution and is used as the reference ice sheet surface elevation to account for the surface slope of the glaciers. Because the repeating passes of ICESat-2 do not exactly survey the same location on the surface of the ice sheet (particularly in the first 9 months of the ICESat-2 mission), ATL06 measurements from season to season are affected by both the vertical component of surface elevation change and differences in surface elevation due to surface slope. To account for this, we sampled the ArcticDEM at each ATL06 measurement and subtracted the ArcticDEM elevation from each ATL06 surface elevation measurement. This effectively changes the datum of the ATL06 measurements to that of the ArcticDEM, thereby accounting

for the surface slope of the ice sheet within our bounding boxes, leaving just the vertical component of surface elevation differences.

We use the ATL06 data within each bounding box, a surface mass balance model, and a firn model to calculate each glacier's dynamic thickness change from season to season. For each glacier, we calculate the surface elevation change (dH) between ICESat-2 observations and the ArcticDEM. We then calculated the seasonal dynamic dH as the mean of the dH values within each bounding box for each year and season, and we subtracted the surface elevation change due to changes in surface mass balance (SMB) and firn air content changes using output from the Community Firn Model (CFM; Medley et al., 2020), forced by Modern-Era Retrospective analysis for Research and Applications, Version 2 (MERRA-2) climate reanalysis (Gelaro et al., 2017). Over the 2-year timescale of our study, we assumed constant bed elevation, and, thus, our surface elevation change measurements are equal to ice thickness change. We removed the trend from each glacier's seasonal dynamic dH, calculated over the entire duration of the available data to isolate the seasonal fluctuations from the longer-term trend. We removed 5 of the 42 glaciers with measurements of seasonal dynamic dH larger than 50 m over one season, assuming that these are errors (Joughin et al., 2020), leaving 37 glaciers for which we classified seasonal dynamic dH patterns.

To account for uncertainty in seasonal dynamic dH, we propagated error through our calculations from each data source with the assumption of random, uncorrelated error. We used the error estimates provided by ATL06 to account for error on each height data point (h_sigma). We conservatively assume 5 m of random error in the ArcticDEM elevations, although the actual uncertainty in ArcticDEM elevations is likely less than this value (Noh and Howat, 2015). We assume a 20 % uncertainty on the thickness change due to SMB and firn components, estimated by the CFM. Assuming uncorrelated and random errors in the ATL06 and ArcticDEM surface elevation measurements, we used standard error propagation rules to calculate the error on seasonal dynamic dH, which is $\sigma_{\text{s.d.d}H}$:

$$\sigma_{\text{s.d.d}H} = \frac{1}{n}\left(\sum_{i=1}^{n}\sigma_{\text{h\_li},i}^2 + 5^2\right)^{1/2} + 02 \times |dH_{\text{CFM}}|, \quad (1)$$

where $\sigma_{\text{h\_li},i}$ represents the error on each ATL06 surface elevation measurement (h_li_sigma), 5 m represents the error in each ArcticDEM surface elevation, n represents the number of ATL06 elevations within the bounding box for a particular season, and dH_{CFM} is the absolute value of the magnitude of surface elevation change due to changes in SMB and firn air content changes from CFM. We do not account for uncertainty in the trend that is removed from each glacier's seasonal dynamic dH because the trend is removed solely to present the thickness changes more clearly in plots. Quantifying uncertainty in the trend of dynamic thickness change

could be done more thoroughly in future studies, given that more ICESat-2 data will be collected over the coming years. Additionally, keeping the trend in the seasonal dynamic dH has no impact on our categorization of glacier behavior for all but five glaciers, as we discuss in Sect. 4.

Using the time series of seasonal dynamic dH for each glacier, we manually grouped glaciers into categories based on their seasonal patterns of thickness change. Because seasonal dynamic dH had not been surveyed for a representative set of GrIS outlet glaciers, we did not prescribe categories prior to generating results. Instead, we based the categories on the timing of observed seasonal dynamic thinning and thickening for our surveyed glaciers. These classifications are based on the difference from one season to the next, rather than at each point in time. Each year of data is individually categorized; in other words, the classification for one glacier in 2019 does not influence the classification of the same glacier in 2020.

3 Results

We find that, over 2019 and 2020, the 37 surveyed glaciers can be categorized into seven seasonal patterns: no statistically significant change, mid-year thinning, mid-year thickening, winter-to-spring and summer-to-autumn thinning with spring-to-summer thickening, spring-to-summer thinning with winter-to-spring and summer-to-autumn thickening, sharp single-season thickening, and full-year thickening (Fig. 1). Glaciers were classified as "no statistically significant change" if uncertainties of seasonal dynamic dH were larger than the amplitude of seasonal change across all seasons within a given year. Sharp single-season thickening includes glaciers that undergo a lone season of significant (> 3 times the change between any other seasons and > 3 times the uncertainties for that glacier) thickening (either spring or summer) followed immediately by a similar sharp decline in thickness. Rink Isbræ is the best example of this, undergoing 6–10 m of change during this spike (Fig. 1e). Mid-year thickening refers to glaciers exhibiting two consecutive seasons of winter-to-spring and spring-to-summer thickening before summer-to-autumn thinning. Conversely, glaciers with mid-year thinning exhibit winter-to-spring and spring-to-summer thinning with summer-to-autumn thickening. Each glacier's detrended dynamic thickness change, alongside the seasonal trend of SMB and total dH change, is plotted in the Supplement (Figs. S1 through S34). Although we have removed the trend to better illustrate seasonal dynamic dH for each glacier, we note that keeping the trend in the data alters our classifications for just five of the surveyed glaciers: Alanngorliup Sermia (Fig. S1), Kangerlussuup Sermia (Fig. S9), Kakivfaat Sermiat (Fig. S13), Cornell Gletsjer (Fig. S17), and Nansen Gletsjer (Fig. S22). Without the trend removed from the dynamic dH, there is a thinning trend in 2019 for Kangerlussuup Sermia (Fig. S9) and Kakiv-
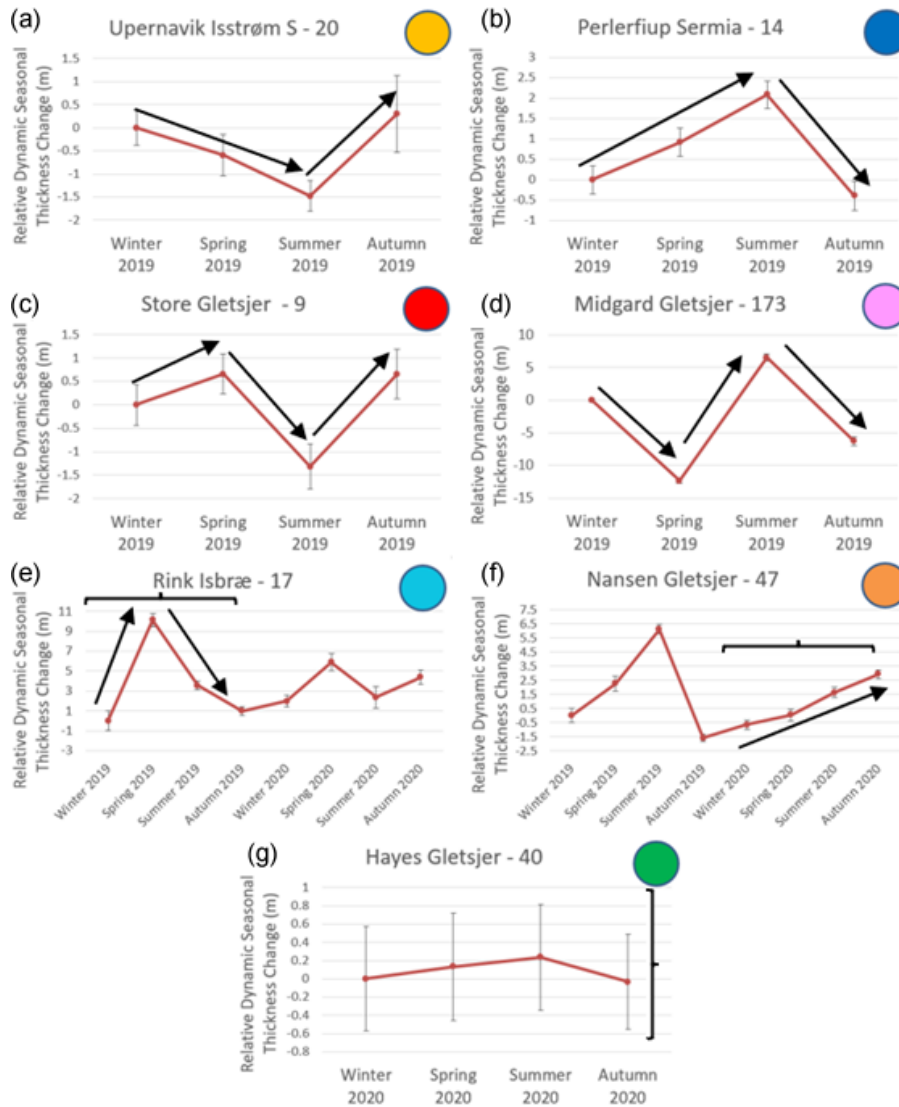
Figure 1. Patterns of outlet glacier dynamic seasonal thickness change with annual trend removed: **(a)** mid-year thinning, **(b)** mid-year thickening, **(c)** summer thinning with spring and autumn thickening, **(d)** spring and autumn thinning with summer thickening, **(e)** sharp single-season thickening, **(f)** full-year thickening, and **(g)** no statistically significant change. Curly brackets highlight **(f)** the full-year thickening pattern of Nansen Gletsjer in 2020 and **(g)** the extent of the error bars encompassing no seasonal change for Hayes Gletsjer. Each value plotted is relative to the first value in the time series, which is shifted to zero.

faat Sermiat (Fig. S13), across both years for Cornell Gletsjer (Fig. S17), and in 2020 for Nansen Gletsjer (Fig. S22). Alanngorliup Sermia (Fig. S1) exhibits a slight overall thickening. These glaciers exhibit strong 1-to-2-year trends, and although, for example, there is little seasonal change over 2019 for Kangerlussuup Sermia in their detrended seasonal dynamic dH values, the glacier is actually thinning overall across throughout the year without the annual trend removed. What this does highlight is that for all other glaciers, their seasonal dynamic thickness changes during at least one season are larger in magnitude than changes due to the 1- or 2-year trend, and, thus, our classification is not sensitive to the removal of the trend. That being said, in general, care must be taken when interpreting seasonal changes with a trend removed that have been estimated from just 1 or 2 years of data.

We find that the 37 surveyed GrIS outlet glaciers are well distributed across the seven patterns. Figure 2 shows glacier classifications for both 2019 and 2020 in the table but displays the classification from the earliest available year on the map. With each year individually categorized, there are 51 total seasonal cycles observed between 2019 (30) and 2020 (21). Of these seasonal cycles, there are 15 seasonal cycles that exhibit spring-to-summer thickening with winter-
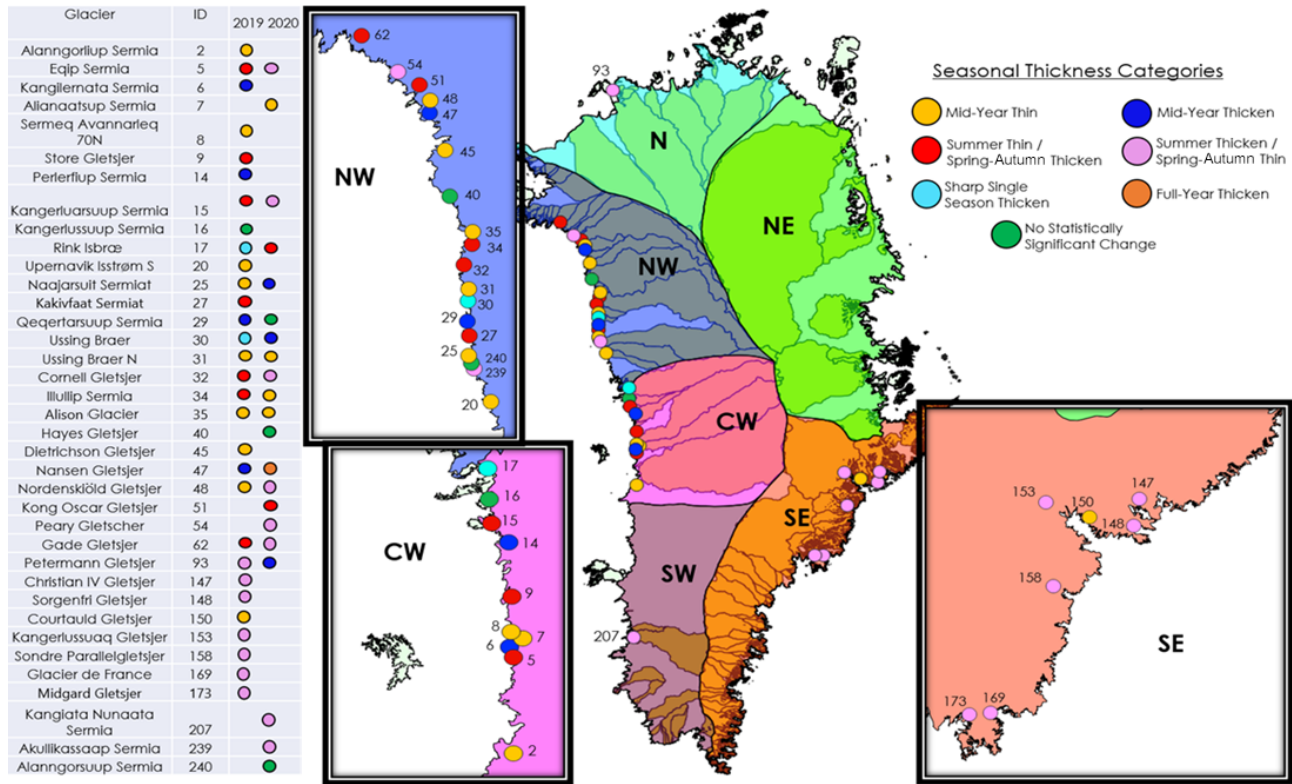
Figure 2. Locations, patterns of seasonal dynamic thickness change, and average ice speeds of 37 GrIS outlet glaciers. Glaciers with different patterns in 2019 and 2020 are depicted on the ice sheet map with their 2019 pattern coloration, while both 2019 and 2020 patterns are shown in their yearly pattern in the left-side table.

to-spring and summer-to-autumn thinning, 13 seasonal cycles that experience mid-year thinning, 9 seasonal cycles within the pattern of spring-to-summer thinning and winter-to-spring and summer-to-autumn thickening, 7 seasonal cycles with mid-year thickening, 2 seasonal cycles with sharp single-season thickening, 1 seasonal cycle exhibiting full-year thickening, and 4 seasonal cycles with a pattern of no statistically significant change. Of the 14 glaciers for which we have 2 years of data, we find that most glaciers exhibit patterns of seasonal thickness change that differ from year to year. Two glaciers exhibit repeating patterns: Ussing Braer N (Fig. S31) and Alison Glacier (Fig. S35). However, the remaining glaciers, for which ICESat-2 can so far provide two annual cycles worth of data, exhibit changing patterns between 2019 and 2020.

Although there are spatial clusters of glaciers with similar patterns of seasonal thickness change, there is heterogeneity within the regions that contain multiple surveyed glaciers (Fig. 2). We use the 2019 classifications, for all glaciers with data in 2019, to compare glaciers per region because we have more glaciers classified in that year (30 glaciers) than in 2020. In the northwest, six glaciers exhibit a mid-year thinning pattern, five glaciers exhibit spring-to-summer thinning with winter-to-spring and summer-to-autumn thicken-

ing, two exhibit spring-to-summer thickening with winter-to-spring and summer-to-autumn thinning, two exhibit mid-year thickening, one glacier exhibits sharp single-season thickening, and two exhibit no statistically significant change. In the central-western region, three glaciers exhibit spring-to-summer thinning with winter-to-spring and summer-to-autumn thickening, three glaciers exhibit mid-year thinning, two glaciers exhibit mid-year thickening, one glacier exhibits sharp single-season thickening, and one glacier exhibits no statistically significant change. Within the southeast, six glaciers exhibit spring-to-summer thickening with winter-to-spring and summer-to-autumn thinning and one glacier exhibits a mid-year thinning pattern. In the north, the single surveyed glacier, Petermann Gletsjer, exhibits spring-to-summer thickening with winter-to-spring and summer-to-autumn thinning in 2019 but switches to mid-year thickening in 2020. Small clusters of neighboring glaciers with similar patterns can be seen in the northwest with some form of mid-year or summer thinning (glacier IDs 31, 32, 34, and 35) and the central-western region (glacier IDs 5, 7, 8, and 9), and the southeast presents the most homogeneity, with six glaciers exhibiting the same pattern (glacier IDs 147, 148, 153, 158, 169, and 173), but there is no one pattern that is representative of all glaciers within each region.

4   Discussion and conclusions

Enabled by 91 d repeat measurements from ICESat-2, we have developed the first classification of GrIS outlet glacier patterns of seasonal dynamic thickness change for a representative sample of glaciers from around the ice sheet. We have chosen to use the ATL06 data product and to account for along- and across-track surface slopes using the ArcticDEM as a reference elevation dataset. This method allowed us to aggregate surface elevation data within customized bounding boxes, representative of each glacier's behavior. Higher-level data products, such as ATL11 and ATL15, will provide estimates of surface elevation change through time, and we believe it will be worthwhile for future work to compare our results against the higher-level ICESat-2 products, both to build confidence in our results and as a check on the data products themselves.

Our results reveal little regional coherency in patterns of seasonal dynamic thickness change, outside of the southeastern region, indicating that mesoscale atmospheric-circulation patterns are not the likely driver of differences in patterns among glaciers. While we do find small clusters of similar patterns, we do not observe similar patterns across the larger northwestern or central-western ice sheet regions. If atmospheric forcing (or errors in our model for the atmospheric forcing) were the primary driver of seasonal dynamic thickness changes, we would expect to see coherent patterns of seasonal changes across each region. However, we do not find this to be the case, indicating that other factors that differ from glacier to glacier within each region are causing the differences in observed patterns. This finding is consistent with seasonal glacier velocity changes, which also exhibit spatial heterogeneity (Moon et al., 2014; Vijay et al., 2019, 2021). Ocean forcing may be responsible for the differences in patterns of seasonal dynamic thickness change because heat transport from the continental shelf to the termini of outlet glaciers is modulated by fjord geometry, which is heterogeneous among glaciers (Carroll et al., 2017). Each glacier's unique geometry, including both fjord geometry and subglacial bed topography, which have been shown to govern observed differences in terminus retreat (Catania et al., 2018), and the multi-annual upstream diffusion of thinning (Felikson et al., 2021), may also be responsible for the observed heterogeneity in seasonal thickness changes. Additionally, glacier geometry may influence each glacier's dynamic seasonal response by modulating the effects of changes in driving stress and surface melt, driven by atmospheric forcing.

Refining the ATL06 data quality flag (atl06_quality_summary), with the goal of accepting additional good-quality measurements that are currently flagged as poor-quality, would benefit future studies of seasonal outlet glacier change by increasing the data volume available. Because ICESat-2 has a repeat cycle of 91 d, collecting good-quality data from each pass is critical to studies of the seasonal thickness changes of outlet glaciers.

The current set of parameters used by the ATL06 quality summary flag may remove good-quality measurements over rough topography, high surface slopes, or low-reflectivity surfaces under clouds (Smith et al., 2021). In the course of our study, we found that 12 additional glaciers, of the subset of 65 glaciers we initially selected from the MEaSUREs dataset, could be included in our results, had we ignored the quality summary flag entirely. Of course, some of the measurements that are removed by the quality summary flag are unusable, and we do not advocate ignoring data quality checks entirely. However, we suggest that further inspection of the parameters used for the quality summary flag to potentially reduce the strictness by which data are eliminated may prove useful and would allow additional glaciers to be considered in future ICESat-2 data releases.

As ICESat-2 continues data collection, future work should build on our 2-year assessment of seasonal dynamic thickness changes by extending our record and comparing it with other glacier variables and external forcings. The MEaSUREs dataset identifies 239 total outlet glaciers around the ice sheet, and, by adding more outlet glaciers and extending the record forward in time, future studies can examine how consistent the patterns are from year to year, identify new patterns not exhibited by the glaciers in our study, and better identify glaciers that exhibit the same or different patterns through time. With a longer and more comprehensive classification of seasonal thickness changes, future work can focus on compiling a holistic record of seasonal glacier dynamics by investigating thickness changes together with terminus position and velocity changes. The subset of glaciers that we have selected for study are ones that have a temporally rich dataset of terminus position changes from the newly developed CALFIN automated deep learning extraction method (Cheng et al., 2021) as well as from added sources in the recent TermPicks (Goliber et al., 2021) dataset, which will allow our results to be directly compared with seasonal terminus positions once CALFIN data are extended into late 2019 and 2020. Finally, to advance our understanding of the processes that drive seasonal glacier behavior, future work should compare seasonal dynamic thickness changes with external forcings such as seasonal ocean temperature changes and surface meltwater runoff estimates. Our study provides the first classification of seasonal dynamic thickness changes of outlet glaciers around the GrIS to complement previous classifications of seasonal velocity change (Moon et al., 2014; Vijay et al., 2019, 2021), bringing us one step closer to a holistic understanding of seasonal glacier dynamics.

Firn Model and MERRA-2. Additionally, a shapefile of locations of the glaciers surveyed is provided.

References

Carroll, D., Sutherland, D. A., Shroyer, E. L., Nash, J. D., Catania, G. A., and Stearns, L. A.: Subglacial discharge-driven renewal of tidewater glacier fjords, J. Geophys. Res.-Oceans, 125, 2293, https://doi.org/10.1002/grl.50825, 2017.

Catania, G. A., Stearns, L. A., Sutherland, D. A., Fried, M. J., Bartholomaus, T. C., Morlighem, M., Shroyer, E., and Nash, J.: Geometric Controls on Tidewater Glacier Retreat in Central Western Greenland, J. Geophys. Res.-Earth Surf., 29, 1–15, https://doi.org/10.1029/2017JF004499, 2018.

Cheng, D., Hayes, W., Larour, E., Mohajerani, Y., Wood, M., Velicogna, I., and Rignot, E.: Calving Front Machine (CALFIN): glacial termini dataset and automated deep learning extraction method for Greenland, 1972–2019, The Cryosphere, 15, 1663–1675, https://doi.org/10.5194/tc-15-1663-2021, 2021.

Choi, Y., Morlighem, M., Rignot, E., and Wood, M.: Ice dynamics will remain a primary driver of Greenland ice sheet mass loss over the next century, Commun. Earth Environ., 2, 26, https://doi.org/10.1038/s43247-021-00092-z, 2021.

Church, J. A., Clark, P. U., Cazenave, A., Gregory, J. M., Jevrejeva, S., Levermann, A., Merrifield, M. A., Milne, G. A., Nerem, R. S., Nunn, P. D., Payne, A. J., Pfeffer, W. T., Stammer, D., and Unnikrishnan, A. S.: Sea Level Change, in: Climate Change 2013: The Physical Science Basis. Contribution of Working Group I to the Fifth Assessment Report of the Intergovernmental Panel on Climate Change, edited by: Stocker, T. F., Qin, D., Plattner, G.-K., Tignor M., Allen, S. K., Boshung, J., Nauels, A., Xia, Y., Bex, V., and Midgley, P. M., Cambridge University Press, Cambridge, United Kingdom and New York, NY, USA, https://doi.org/10.1017/CBO9781107415324.026, 2013.

Felikson, D., Catania, G. A., Bartholomaus, T. C., Morlighem, M., and Noël, B. P. Y.: Steep Glacier Bed Knickpoints Mitigate Inland Thinning in Greenland, Geophys. Res. Lett., 48, e2020GL090112, https://doi.org/10.1029/2020GL090112, 2021.

Gelaro, R., McCarty, W., Suárez, M. J., Todling, R., Molod, A., Takacs, L., Randles, C. A., Darmenov, A., Bosilovich, M. G., Reichle, R., Wargan, K., Coy, L., Cullather, R., Draper, C., Akella, S., Buchard, V., Conaty, A., da Silva, A. M., Gu, W., Kim, G., Koster, R., Lucchesi, R., Merkova, D., Nielsen, J. E., Partyka, G., Pawson, S., Putman, W., Rienecker, M., Schubert, S. D., Sienkiewicz, M., and Zhao, B.: The Modern-Era Retrospective Analysis for Research and Applications, Version 2 (MERRA-2), J. Climate, 30, 5419–5454, 2017.

Goliber, S., Black, T., Catania, G., Lea, J. M., Olsen, H., Cheng, D., Bevan, S., Bjørk, A., Bunce, C., Brough, S., Carr, J. R., Cowton, T., Gardner, A., Fahrner, D., Hill, E., Joughin, I., Korsgaard, N., Luckman, A., Moon, T., Murray, T., Sole, A., Wood, M., and Zhang, E.: TermPicks: A century of Greenland glacier terminus data for use in machine learning applications, The Cryosphere Discuss. [preprint], https://doi.org/10.5194/tc-2021-311, in review, 2021.

Gray, L., Burgess, D., Copland, L., Langley, K., Gogineni, P., Paden, J., Leuschen, C., van As, D., Fausto, R., Joughin, I., and Smith, B.: Measuring height change around the periphery of the greenland ice sheet with radar altimetry, Front. Earth Sci., 7, 146, https://doi.org/10.3389/feart.2019.00146, 2019.

Johannessen, O. M., Khvorostovsky, K., Miles, M. W., and Bobylev, L. P.: Recent Ice-Sheet Growth in the Interior of Greenland, Science, vol. 310, no. 5750, American Association for the Advancement of Science, 1013–1016, https://doi.org/10.1126/science.1115356, 2005.

Joughin, I., Moon, T., Joughin, J., and Black, T.: MEaSUREs Annual Greenland Outlet Glacier Terminus Positions from SAR Mosaics, Version 1. Boulder, Colorado USA. NASA National Snow and Ice Data Center Distributed Active Archive Center [data set], https://doi.org/10.5067/DC0MLBOCL3EL, 2015, 2017.

Joughin, I., Shean, D. E., Smith, B. E., and Floricioiu, D.: A decade of variability on Jakobshavn Isbræ: ocean temperatures pace speed through influence on mélange rigidity, The Cryosphere, 14, 211–227, https://doi.org/10.5194/tc-14-211-2020, 2020.

Markus, T., Neumann, T., Martino, A., Abdalati, W., Brunt, K., Csatho, B., Farrell, S., Fricker, H., Gardner, A., Harding, D., Jasinski, M., Kwok, R., Magruder, L., Lubin, D.,

Luthcke, S., Morison, J., Nelson, R., Neuenschwander, A., Palm, S., Popescu, S., Shum, C. K., Schutz, B., Smith, B., Yang, Y., and Zwally, J.: The Ice, Cloud, and land Elevation Satellite-2 (ICESat-2): Science requirements, concept, and implementation, Remote Sens. Environ., 190, 260–273, https://doi.org/10.1016/j.rse.2016.12.029, 2017.

McMillan, M., Leeson, A., Shepherd, A., Briggs, K., Armitage, T. W. K., Hogg, A., Munneke, P. K., van den Broeke, M., Noël, B., van de Berg W. J., Ligtenberg, S., Horwath, M., Groh, A., Muir, A., and Gilbert, L.: A high-resolution record of Greenland mass balance, Geophys. Res. Lett., 43, 7002–7010, https://doi.org/10.1002/2016GL069666, 2016.

Medley, B., Neumann, T. A., Zwally, H. J., and Smith, B. E.: Forty-year Simulations of Firn Processes over the Greenland and Antarctic Ice Sheets, The Cryosphere Discuss. [preprint], https://doi.org/10.5194/tc-2020-266, in review, 2020.

Moon, T., Joughin, I., Smith, B., van den Broeke, M. R., van de Berg, W. J., Noël, B., and Usher, M.: Distinct patterns of seasonal Greenland glacier velocity, Geophys. Res. Lett., 41, 7209–7216, https://doi.org/10.1002/2014GL061836, 2014.

Mouginot, J., Rignot, E., Bjørk, A., van den Broeke, M., Millan, R., Morlighem, M., Noël, B., Scheuchl, B., and Wood, M.: Forty-Six Years of Greenland Ice Sheet Mass Balance from 1972 to 2018, P. Natl. Acad. Sci. USA, 116, 9239, https://doi.org/10.1073/pnas.1904242116, 2019.

Neumann, T. A., Martino, A. J., Markus, T., Bae, S., Bock, M.R., Brenner, A. C., Brunt, K. M., Cavanaugh, J., Fernandes, S.T., Hancock, D. W., Harbeck, K., Lee, J., Kurtz, N. T., Luers,P. J., Luthcke, S. B., Magruder, L., Pennington, T. A., Ramos-Izquierdo, L., Rebold, T., Skoog, J., and Thomas, T. C.: The Ice,Cloud, and Land Elevation Satellite – 2 mission: A global geolo-cated photon product derived from the Advanced Topographic Laser Altimeter System, Remote Sens. Environ., 233, 111325, https://doi.org/10.1016/j.rse.2019.111325, 2019.

Noh, M. J. and Howat, I. M.: Automated stereo-photogrammetric DEM generation at high latitudes: Surface Extraction with TIN-based Search-space Minimization (SETSM) validation and demonstration over glaciated regions, GIScience Remote Sens,, 52, 198–217, https://doi.org/10.1080/15481603.2015.1008621, 2015.

Oppenheimer, M., Glavovic, B. C., Hinkel, J., van de Wal, R., Magnan, A. K., Abd-Elgawad, A., Cai, R., Cifuentes-Jara, M., DeConto, R. M., Ghosh, T., Hay, J., Isla, F., Marzeion, B., Meyssignac, B., and Sebesvari, Z.: Sea Level Rise and Implications for Low-Lying Islands, Coasts and Communities, in: IPCC Special Report on the Ocean and Cryosphere in a Changing Climate, edited by: Pörtner, H.-O., Roberts, D. C., Masson-Delmotte, V., Zhai, P., Tignor, M., Poloczanska, E., Mintenbeck, K., Alegría, A., Nicolai, M., Okem, A., Petzold, J., Rama, B., and Weyer, N. M., IPCC Special Report on the Ocean and Cryosphere in a Changing Climate, 126, in press, https://www.ipcc.ch/site/assets/uploads/sites/3/2019/11/08_SROCC_Ch04_FINAL.pdf (last access: 30 March 2022), 2019.

Porter, C., Morin, P., Howat, I., Noh, M. J., Bates, B., Peterman, K., Keesey, S., Schlenk, M., Gardiner, J., Tomko, K., Willis, M., Kelleher, C., Cloutier, M., Husby, E., Foga, S., Nakamura, H., Platson, M., Wethington, M. Jr., Williamson, C., Bauer, G., Enos, J., Arnold, G., Kramer, W., Becker, P., Doshi, A., D'Souza, C., Cummens, P., Laurier, F., and Bojesen, M.: "ArcticDEM", Harvard Dataverse [data set], V1, https://doi.org/10.7910/DVN/OHHUKH, 2018.

Rignot, E. and Mouginot, J.: Ice flow in Greenland for the International Polar Year 2008–2009, Geophys. Res. Lett., 39, L11501, https://doi.org/10.1029/2012GL051634, 2012.

Smith, B., Fricker, H. A., Holschuh, N., Gardner, A. S., Adusumilli, S., Brunt, K. M., Csatho, B., Harbeck, K., Huth, A., Neumann, T., Nilsson, J., and Siegfried, M. R.: Land Ice Height-Retrieval Algorithm for NASA's ICESat-2 Photon-Counting Laser Altimeter, Remote Sens. Environ., 233, 111352, https://doi.org/10.1016/j.rse.2019.111352, 2019.

Smith, B., Fricker, H. A., Gardner, A., Siegfried, M. R., Adusumilli, S., Csathó, B. M., Holschuh, N., Nilsson, J., Paolo, F. S., and the ICESat-2 Science Team.: ATLAS/ICESat-2 L3A Land Ice Height, Version 3, Boulder, Colorado USA, NASA National Snow and Ice Data Center Distributed Active Archive Center [data set], https://doi.org/10.5067/ATLAS/ATL06.003, 2020.

Smith, B. E., Harbeck, K., Roberts, L., Neumann, T., Brunt, K., Fricker, H. A., Gardner, A., Seigfried, M. R., Adusumilli, S., Csatho, B. M., Holschuh, N., Nilsson, J., and Paolo, F. S.: ICESat-2 Algorithm Theoretical Basis Document (ATBD) for Land Ice Along- Track Height (ATL06), Applied Physics Laboratory, University of Washington, Seattle, WA, https://icesat-2.gsfc.nasa.gov/science/data-products (last access: 30 March 2022), 2021.

Sutterley, T. C., Velicogna, I., Fettweis, X., Rignot, E., Noel, B., and van den Broeke, M. R: Evaluation of reconstructions of snow/ice melt in Greenland by regional atmospheric climate models using laser altimetry data, Geophys. Res. Lett., 45, 8324–8333, https://doi.org/10.1029/2018GL078645, 2018.

Vijay, S., Khan, S. A., Kusk, A., Solgaard, A. M., Moon, T., and Bjørk, A. A.: Resolving Seasonal Ice Velocity of 45 Greenlandic Glaciers With Very High Temporal Details, Geophys. Res. Lett., 46, 1485–1495, https://doi.org/10.1029/2018GL081503, 2019.

Vijay, S., King, M., Howat, I., Solgaard, A., Khan, S., and Noël, B.: Greenland ice-sheet wide glacier classification based on two distinct seasonal ice velocity behaviors, J. Glaciol., 67, 1241–1248, https://doi.org/10.1017/jog.2021.89, 2021.